Measuring the strongest chemical bond with spectroscopic accuracy: CO bond-dissociation energy via predissociation of superexcited states

Shiyan Gong, Peng Wang, and Yuxiang Mo*

Department of Physics and State Key Laboratory of Low-Dimensional Quantum Physics, Tsinghua University, Beijing 100084, China

(Received 31 July 2023; accepted 21 September 2023; published 9 October 2023)

The chemical bond of carbon monoxide (CO) is the strongest bond. It plays a crucial role in thermochemistry and serves as a benchmark for electronic structure calculations. The most accurate value to date has been obtained by analyzing its predissociation spectra related to the lowest energy dissociation channel, achieving an uncertainty of 6 cm^{-1}. In this work, we measured the bond-dissociation energy of CO by recording the CO rotationally resolved, sharp-rising the $C(^1D_2)$ fragment yield spectrum related to the $C(^1D_2) + O(^1D_2)$ threshold. The sharp rising steps at the thresholds in the fragment yield spectrum are caused by the predissociation of broad vibronic bands of superexcited states. The thresholds were validated by the velocity map images of the $C(^1D_2)$. The determined bond-dissociation energy is 89 602.80 ($\pm$0.10) cm^{-1}, representing an improvement in accuracy of over one order of magnitude compared to the previous values.

DOI: 10.1103/PhysRevA.108.042802

I. INTRODUCTION

Carbon monoxide (CO) is the second most abundant molecule in the universe after H_2 and is known to have the strongest chemical bond, with a bond-dissociation energy (BDE) of approximately 11.11 eV [1–7]. The BDE of CO is critical in thermochemistry as it relates to the formation enthalpies of the carbon and oxygen atoms, which are the building blocks of all organic molecules [8]. It also serves as a benchmark for electronic structure calculations involving electron correlations [9]. Despite the BDE of CO being measured as early as 1934, and numerous spectroscopists working to improve its accuracy, the uncertainty still remains at 6 cm^{-1} [1–7]. In contrast, the BDE of H_2 has been measured with high accuracy better than 10^{-5} cm^{-1} [10–14]. Therefore, there is a need for a more accurate determination of the BDE of CO, especially at a spectroscopic accuracy level (better than 1 cm^{-1}).

The previous measurements of the BDE of CO were primarily focused on observing its predissociations in the $B\,^1\Sigma^+$ Rydberg state, which correlates with its first dissociation threshold. These studies utilized an empirical model that requires determining energy levels of the highest non-predissociated and lowest predissociated rotational states. The accuracy of the BDE value obtained through this model depends on several factors, including the number of measured isotopologue energy levels and the energy spacings between them. Typically, these energy spacings range from 50 to 140 cm^{-1}. In 1955, Douglas and Møller [4] conducted a study using two isotopologues and four pairs of energy levels, resulting in an uncertainty of 30 cm^{-1} for the BDE value. In 2014, Kepa *et al.* [7] expanded upon this by utilizing eight isotopologues and 13 pairs of rovibronic energy levels, reducing the uncertainty to 6 cm^{-1}. However, it is clear that further enhancing the accuracy of the BDE using this model could present challenges.

Another highly accurate method for measuring the BDE is to determine the threshold of ion-pair dissociation [15–18]. This approach involves measuring the ion pair yield spectrum near the dissociation threshold or the spectrum of fragment ions with zero kinetic energies. It has proven successful in studying molecules such as O_2, F_2, Cl_2, HCl, and H_2S [15–18]. However, achieving an accuracy better than 1 cm^{-1} using this method is challenging due to the influence of the resident electric field in the instrument, which can lower the ion-pair dissociation threshold and is difficult to account for. In the case of CO, another challenge is that the ion-pair production threshold is near 21 eV [19], and high-resolution lasers near this energy range are rarely available. Therefore, it is difficult to use the ion-pair spectral method to measure the BDE of CO with spectroscopic accuracy.

The BDE can also be accurately determined by analyzing the fragment yield spectrum near the threshold in direct dissociation. However, the direct dissociation cross section at the threshold is typically small due to unfavorable Franck-Condon factors and the requirement of the Wigner threshold law for the short-range interaction potential [20,21]. Nevertheless, H_2 is one of the few exceptions where direct dissociation has a large cross section at the threshold. Its BDE has been successfully measured by analyzing the $H(2l)$ fragment yield spectra at the second dissociation threshold [10–14].

Molecular excited states with internal energies higher than the ionization energy are called superexcited states, typically in the form of molecular Rydberg states with vibronically excited ionic cores [22,23]. Excitation to a Rydberg state can be strong due to favorable Franck-Condon factors. These superexcited states can strongly couple the dissociation and ionization continua. In other words, superexcited states often have broad resonance widths due to their short lifetimes. Unlike direct dissociation, where the Wigner threshold law states that the dissociation cross section must be

*ymo@mail.tsinghua.edu.cn

zero at the threshold for diatomic molecules with short-range interaction potential [21], the predissociation of the superexcited state can have a nonzero cross section even at the threshold.

For the CO molecule, its dissociation cross sections in the superexcited energy region have previously been determined by subtracting the ionization cross section from the total absorption cross section [24,25]. These studies have revealed that the dissociation cross sections exhibit a continuous variation around 14.34 eV, which is close to the threshold energy of the $C(^1D_2) + O(^1D_2)$ channel. This suggests that investigating the predissociation of CO within this energy range could provide a useful approach to measure the dissociation threshold. While recent studies have explored the dissociation of CO Rydberg states, there is currently a lack of data on the state-resolved fragment yield spectra of the $C(^1D_2)$ fragments in this specific energy region [26,27].

In this work, we present our findings on the fragment yield spectrum of the $C(^1D_2)$ near the threshold of the $C(^1D_2) + O(^1D_2)$. One notable observation is the sharp increase in the $C(^1D_2)$ fragment signals at the dissociation thresholds, which are due to the predissociations of superexcited states. As a result, we have determined the BDE of CO to be $89\,602.80(\pm0.10)\,\mathrm{cm}^{-1}$.

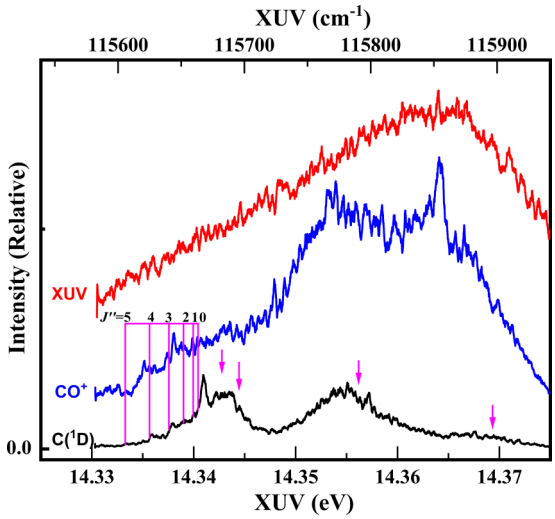

FIG. 1. Photoionization yield spectrum of CO, fragment yield spectrum of the $C(^1D_2)$ from the photodissociation of CO, and the XUV light intensities as a function of photon energies. The arrows indicate the energy positions where the velocity map images of the $C(^1D_2)$ fragments were measured (see Fig. 2). The spectra were not normalized to XUV light intensities, and the relative signals among different spectra were also not normalized.

II. EXPERIMENTAL METHOD

Our experimental setup consists of a tunable extreme UV (XUV) laser pump (~86.5 nm; ~10 nJ per pulse; repetition rate, 20 Hz), an UV laser probe (320.42 nm, 0.6 mJ), and a standard velocity map imaging apparatus [16,23,28,29]. The XUV laser was generated using a resonance-enhanced four-wave sum mixing scheme ($2\omega_1 + \omega_2$), with two laser beams focused on a pulsed krypton jet. The first laser beam, with a frequency of ω_1, was obtained by tripling the frequency of a dye laser, and the $2\omega_1$ frequency was set to the transition frequency of krypton ($98\,855.07\,\mathrm{cm}^{-1}$) [30]. The second laser beam (ω_2) was scanned between 594 and 598 nm. Both dye lasers were pumped by the same Nd-YAG laser. The bandwidth (full width at half maximum) of our XUV laser was $0.3 \pm 0.05\,\mathrm{cm}^{-1}$, with an absolute frequency accuracy of about $0.1\,\mathrm{cm}^{-1}$. The sum-frequency XUV laser beam was separated from the other beams and focused using a toroidal grating. The probe UV laser beam ionized the $C(1s^2 2s^2 2p^2,\ ^1D_2)$ fragments using the two-photon resonance-enhanced multiphoton ionization method via the Rydberg state the $C(1s^2 2s^2 2p3p,\ ^1D_2)$ [30]. We used LabVIEW software installed on a personal computer to collect ion signals from a digital oscilloscope and scan frequencies (ω_2) from a wavemeter (WS-6; High Finesse Corp., Germany), pulse by pulse. The oscilloscope has a vertical resolution of 12 bits and a bandwidth of 500 MHz, while the wavemeter provides a specified absolute accuracy of $0.02\,\mathrm{cm}^{-1}$. The ions traveled a distance of approximately 1.2 m from the point where the XUV laser and molecular beam crossed to the plane of the microchannel plate detector, which was equipped with a phosphor screen. The acceleration electric voltage for the imaging experiment was set to 1000 V.

III. RESULTS AND DISCUSSION

A. Predissociation mechanism

Figure 1 shows the fragment yield spectrum of the $C(^1D_2)$, the photoionization efficiency (PIE) spectrum of CO, and the intensities of XUV light ranging from 14.330 to 14.375 eV. The velocity map images of the $C(^1D_2)$ fragments were measured at four different excitation energies, indicated by the arrows in Fig. 1. Figure 2(a) displays the inverse Abel transforms of the measured velocity map images. Figure 2(b) and 2(c) shows the corresponding fragment angular distributions and the square of the radius in the images as a function of excitation energies, respectively.

The fragment angular distributions were fitted using the well-known equation [31] $f(\theta) \propto 1 + \beta P_2(\cos\theta)$, where θ represents the angle between the recoil velocity vector and the polarization direction of the dissociation laser, and $P_2(\cos\theta)$ the second-order Legendre polynomial. In the case of direct dissociation of a diatomic molecule, β is 2 or -1 for a parallel or perpendicular transition, respectively. The β values illustrated in Fig. 2(b) are positive; however, much less than the value of 2 for direct dissociations. This suggests a predissociation mechanism involving superexcited states of $^1\Sigma^+$ symmetry. Note that for predissociations near the threshold, as observed in our study, the β values strongly depend on the excitation energies [32].

Previous reports have assigned the absorption and PIE spectra of CO in the studied energy range as Rydberg states converging to the vibrational excited state of $CO^+(X^2\Sigma^+)$ [33–38].

In Fig. 1, the PIE spectrum shows two closely overlapping bands between 14.330 and 14.375 eV. However, in the $C(^1D_2)$ fragment yield spectrum, we are able to distinguish these two bands clearly. The band origins have been

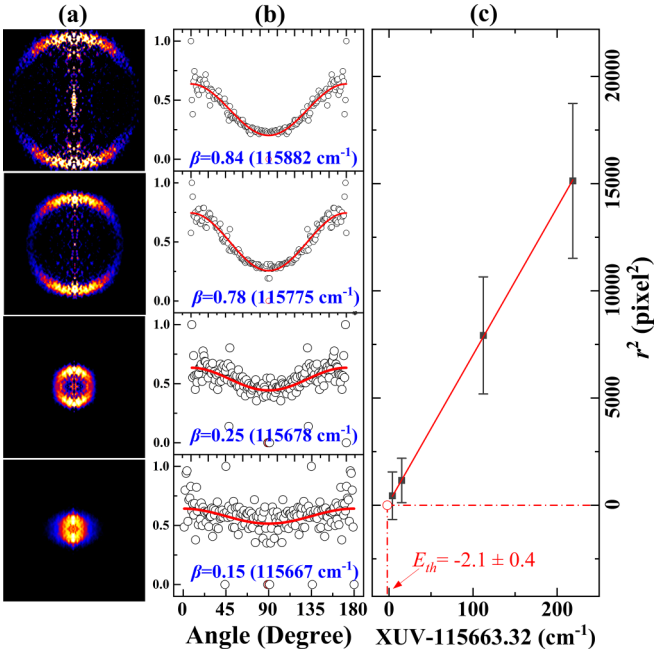

FIG. 2. (a) Inverse Abel transform velocity map images of the $C(^1D_2)$ fragments at four different excitation energies shown in Fig. 1. (b) Corresponding fragment angular distributions and β parameters. (c) The y-axis represents the square of the circle radius measured from the images, labeled as r^2. The translational energies of the fragments in the center of mass are proportional to r^2. The least-squares linear fit extension confirms the dissociation threshold of 115 663.32 cm^{-1} obtained from the $C(^1D_2)$ fragment yield spectrum.

determined to be 14.342 eV (86.448 nm) and 14.355 eV (86.370 nm), respectively, and they have been assigned as Rydberg states with effective quantum numbers $n^* = 4.307$ [converging to $CO^+(X^2\Sigma^+,\ v' = 4)$] and $n^* = 8.323$ [converging to $CO^+(X^2\Sigma^+,\ v' = 2)$], which is consistent with previous reports [35,37,38]. The angular distribution of the $C(^1D_2)$ fragments shows positive β values, confirming that they originate from parallel transitions. Therefore, the two bands can be attributed to Rydberg states $(5\sigma)(5p\sigma)\,^1\Sigma^+$ and $(5\sigma)(9p\sigma)\,^1\Sigma^+$, respectively. These Rydberg states with energies higher than the first ionization energy of CO, also known as superexcited states, can interact with the continuum states of $^1\Sigma^+$ symmetry correlating to the $C(^1D_2) + O(^1D_2)$ threshold. To illustrate the previous discussion more clearly, Fig. 3 shows schematic diabatic potential energy curves of CO with $^1\Sigma^+$ symmetry [39,40], which are related to our work. It can be observed that the excited Rydberg states may interact with the vibrational continua of the $3\,^1\Sigma^+$ and $4\,^1\Sigma^+$ states, which correlate to the limit the $C(^1D_2) + O(^1D_2)$. However, the detailed dynamics should be studied in the future.

The extrapolation of the least-squares linear fit in Fig. 2(c) suggests that the dissociation threshold (intersection with the x-axis) is approximately 2 cm^{-1} lower than the $J'' = 0$ value determined from the $C(^1D_2)$ fragment yield spectrum (discussed later). This is a plausible observation considering that the initial rotational states of the CO molecules were not distinguishable in the images, and the presence of rotationally excited states in the CO beam would lower the apparent

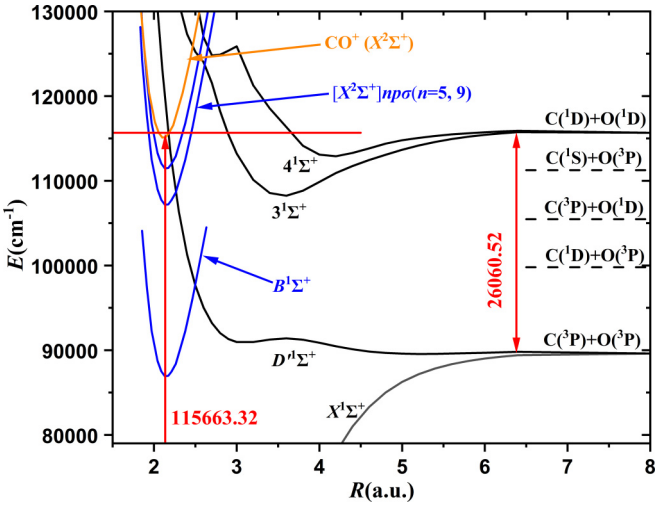

FIG. 3. Schematic diagram for the diabatic potential energy curves (PECs) of CO with $^1\Sigma^+$ symmetry. The PECs for the valency states are adapted from Ref. [39]. The PECs for the CO Rydberg states ($np\sigma\,^1\Sigma^+$ and $B^1\Sigma^+$) are assumed to have a similar shape as the cation $CO^+(X^2\Sigma^+)$; however, the minimum energies are adjusted to the corresponding experimental values [38]. The dissociation limits are also modified to align with the experimental data. Note that the PECs shown in the figure only represent singlet states; channels $C(^1S) + O(^3P)$, $C(^3P) + O(^1D_2)$ and the $C(^1D_2) + O(^3P)$ correlate to triplet states and their PECs are not shown.

dissociation threshold. As a result, the fragment imaging experiments provide evidence supporting the threshold value determined using the fragment yield spectrum discussed next.

B. Dissociation threshold determined from fragment yield spectrum

Figure 4 shows an expanded view of the $C(^1D_2)$ fragment yield spectrum of Fig. 1, revealing six distinct rising steps that are more clearly depicted in the insets. These steps are believed to represent the dissociation thresholds of the $C(^1D_2) + O(^1D_2)$ channel that originate from different rotational states of $CO(X^1\Sigma^+,\ J'' = 0$ to 5). This assignment is supported by two main pieces of experimental evidence:

(1) The measured energy spacings between the six sharp steps in the spectrum coincide with the energy-level spacings between the rotational states of $CO(X^1\Sigma^+)$ within the frequency uncertainty of our instrument (0.1 cm^{-1}). The energy positions of the rotational states from $J'' = 0$ to 5 can be found in Table I. The formula used to calculate the rotational energy levels is $E_{J''} = B_0 J''(J'' + 1)$, with $B_0 = 1.9225\,cm^{-1}$ [5].

(2) We measured the velocity map images of the $C(^1D_2)$ fragments along the sharp steps corresponding to $J'' = 0$, 1, and 3. Several resulting images are presented in Figs. 5(a)–5(c), respectively. For comparison, we also include the velocity map image of the parent molecule CO^+ in Fig. 5(a). The size of the CO^+ image is determined solely by the divergence angle of the CO beam and the size of the focusing spot of the XUV laser. Notably, the diameter of the dots representing the $C(^1D_2)$ fragments at the step locations is approximately two-thirds the size of the CO^+ image. This implies that

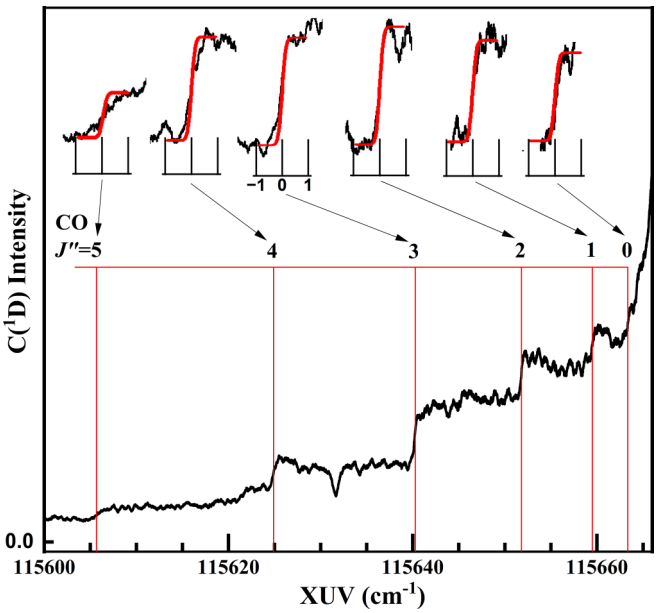

FIG. 4. An expanded view of the C($^1D_2$) fragment yield spectrum of Fig. 1. This spectrum was obtained by averaging ten scans, with each scan consisting of 7000 data points. The insets in the figure provide a closer look at the spectra near the dissociation thresholds for different initial rotational states of CO($X^1\Sigma^+$, J''). The smooth (red) curves represent the simulated spectra, as shown in Fig. 5(d).

the C($^1D_2$) fragments at the steps possess negligible kinetic energies, supporting the conclusion that these steps correspond to the dissociation threshold of CO.

Figs. 5(a)–5(c) also shows the integration of the C($^1D_2$) fragment signals within a small dot (diameter, 20 pixels) at the center of the C($^1D_2$) images as a function of excitation energies for $J'' = 0$, 1, and 3, respectively. The images represent a two-dimensional projection of the fragment velocity distributions. The majority of the fragments within the dots have kinetic energies below 2 cm^{-1}. However, there were some fragments that traveled perpendicular to the detector plate and they may have higher kinetic energies. These fragments are considered background signals and could originate from rotational states above the specified threshold.

The line profiles across the steps in the fragment yield spectrum shown in Figs. 4 and 5, referred to as step profiles, can be simulated by convolving the XUV laser bandwidth (0.3 cm^{-1}) with the assumed step functions for the dissociation cross sections. The step function is defined as $y(x) = 0$ when $x < E_{\text{th}}$ and $y(x) =$ constant when $x \geqslant E_{\text{th}}$, where E_{th} represents the dissociation threshold. Figure 5(d) displays the convolution that nicely reproduces the observed step profiles in Figs. 4 and 5. It is evident that the thresholds are positioned at the centers of the step profiles.

The step width of a step profile refers to the energy difference between the 25% and 75% signal levels at the top of the line profile. In the simulation presented in Fig. 5(d), the step width is approximately 0.17 cm^{-1}. The step widths for different J'' states can be found in Table I. By averaging the step widths for $J'' = 0$, 1, 2, and 3, we obtained an average

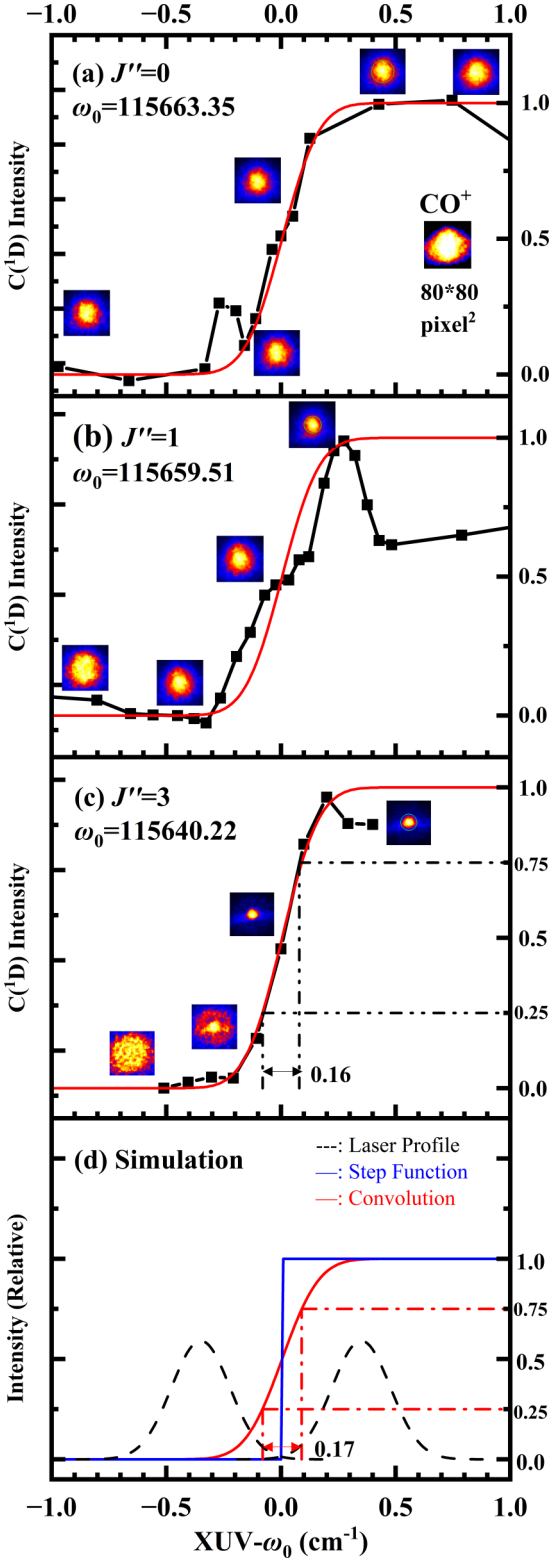

FIG. 5. The fragment yield spectra of the C($^1D_2$) for the dissociation threshold of CO($X^1\Sigma^+$, J''). (a) $J'' = 0$, (b) $J'' = 1$, and (c) $J'' = 3$. The C($^1D_2$) fragment signals were integrated within a ten-pixel-radius circle at the center of the velocity map images. (a) also shows the velocity map image of CO^+. (d) The convolution profile assuming an XUV laser bandwidth of 0.3 cm^{-1} and a step function of dissociation cross section. The smooth (red) curves in (a), (b), and (c) represent the same profile presented in (d).

TABLE I. Measured dissociation thresholds for the $CO(X^1\Sigma^+,\ J'') \rightarrow C(^1D_2) + O(^1D_2)$, as observed in Figs. 4 and 5, and the derived dissociation thresholds for the $CO(X^1\Sigma^+,\ J''=0) \rightarrow C(^1D_2) + O(^1D_2)$ and $C(^3P_0) + O(^3P_2)$. The dissociation channel the $C(^1D_2) + O(^1D_2)$ is 26 060.52 cm^{-1} higher than the lowest energy channel $C(^3P_0) + O(^3P_2)$ [30]. The step width of a step profile refers to the energy difference between the 25% and 75% signal levels at the top of the step profile. The energy unit used in the table is cm^{-1}.

Rotational state	Measured threshold J'' $C(^1D_2) + O(^1D_2)$	Derived threshold $J''=0$ $C(^1D_2) + O(^1D_2)$	Derived threshold $J''=0$ $C(^3P_0) + O(^3P_2)$	Step width J''
		From Fig. 3 (fragment yield spectrum)		
$J''=0$	115 663.32	115 663.320	89 602.800	0.21
$J''=1$	115 659.46	115 663.305	89 602.785	0.26
$J''=2$	115 651.80	115 663.335	89 602.815	0.21
$J''=3$	115 640.23	115 663.300	89 602.780	0.23
$J''=4$	115 624.87	115 663.320	89 602.800	0.47
$J''=5$	115 605.63	115 663.305	89 602.785	0.64
		From Fig. 4 (velocity map images)		
$J''=0$	115 663.35	115 663.350	89 602.830	0.19
$J''=1$	115 659.51	115 663.355	89 602.835	0.31
$J''=3$	115 640.22	115 663.290	89 602.770	0.16
Average[a]		115 663.320	89 602.800	
Standard deviation		0.02	0.02	

[a]The uncertainty for the absolute XUV laser frequency was estimated to be 0.1 cm^{-1}.

value of $0.22 \pm 0.05\ cm^{-1}$. This suggests that the dissociation cross sections exhibit a steplike behavior near the thresholds. Consequently, we can expect to determine the center of the step profile or thresholds with an accuracy of 0.1 cm^{-1}. However, it is important to note that the step widths for $J''=4$ and 5 in Fig. 5 are 0.47 and 0.64 cm^{-1}, respectively, which are larger than 0.17 cm^{-1}. This deviation from the assumption of a step-type cross section may be attributed to a fraction of the spectra originating from direct dissociations that follow the Wigner threshold rule [21]. Further investigation is required for a comprehensive understanding of this phenomenon.

As mentioned earlier, the measured thresholds for different initial rotational states of CO are listed in Table I. Taking into account the statistical analysis of the data and the absolute accuracy of our XUV laser, we have determined the dissociation threshold for the $CO(J''=0) \rightarrow C(^1D_2) + O(^1D_2)$ to be $115\,663.32 \pm 0.10\ cm^{-1}$. It is worth noting that the energy of the $C(^1D_2) + O(^1D_2)$ is 26 060.52 cm^{-1} higher than that of the lowest channel, $C(^3P_0) + O(^3P_2)$ (see Fig. 3) [30]. Consequently, using this information, the BDE of CO is determined to be $89\,602.80 \pm 0.10\ cm^{-1}$.

Table II presents a comparison of the BDE values of CO between our measured value and the previously published data. Our result demonstrates a significant improvement in accuracy, exceeding more than one order of magnitude. It is encouraging to observe that all the data agree within the reported uncertainties, as indicated in Table II [1–7].

IV. CONCLUSION

In this work, we measured the bond-dissociation energy of CO using a combination of XUV laser pump, UV laser probe, and velocity map imaging techniques. The CO rotational state-resolved fragment yield spectrum of the $C(^1D_2)$ revealed distinct steps at the dissociation thresholds, which were identified as the predissociation of CO superexcited states. The dissociation thresholds were further confirmed through the analysis of velocity map images of the $C(^1D_2)$ fragments. The measured bond-dissociation energy of CO was determined to

TABLE II. Bond-dissociation energy (D_0) of CO in units of cm^{-1} and eV.

Authors	D_0 (cm^{-1})	D_0 (eV)[a]	Published year
This work[b]	89 602.80 ± 0.10	11.109 33 ± 0.000 012	2023
Kepa *et al.* [7]	89 597.3 ± 6.0	11.108 6 ± 0.000 7	2014
Eidelsberg *et al.* [6]	89 592 ± 15	11.108 0 ± 0.001 9	1987
Huber and Herzberg [5]	89 447 ± 160	11.09 ± 0.02	1979
Douglas and Møller [4]	89 595 ± 30	11.108 4 ± 0.003 7	1955
Schmid and Gerö [2]	89 620 ± 50	11.111 4 ± 0.006 2	1937

[a]1 eV = 8065.544 cm^{-1}.

[b]The threshold of $C(^1D_2) + O(^1D_2)$ was measured as $115\,663.32 \pm 0.10\ cm^{-1}$ (see Table I), which is 26 060.52 cm^{-1} higher than the lowest dissociation channel $C(^3P_0) + O(^3P_2)$ [30].

be 89 602.80 ($\pm$0.10) cm^{-1} or 11.109 33 ($\pm 1.2 \times 10^{-5}$) eV, representing a significant improvement over the previous values. Our work suggests that this methodology could be utilized to measure bond-dissociation energies of other diatomic or triatomic molecules in future research.

ACKNOWLEDGMENTS

This work was supported by the National Science Foundation of China (Grants No. 21833003 and No. 21773134) and by the National Key R&D Program of China (Grant No. 2018YFA0306504).

[1] D. Coster and F. Brons, Predissociation in the Ångström-bands of CO, Physica **1**, 155 (1934).

[2] R. Schmid and L. Gerö, Über die grenzkurve der dissoziation auf bandenspektroskopischer grundlage, Z. Phys. **104**, 724 (1937).

[3] A. G. Gaydon and W. G. Penney, The dissociation energies of CO, N_2, NO and CN, Proc. Roy. Soc. A **183**, 374 (1945).

[4] A. E. Douglas and C. K. Møller, Predissociations of the $C^{12}O$ and $C^{13}O$ molecules, Can. J. Phys. **33**, 125 (1955).

[5] K. P. Huber and G. Herzberg, *Molecular Spectra and Molecular Structure, Constants of Diatomic Molecules* (Springer, New York, 1979), Vol 4.

[6] M. Eidelsberg, J.-Y. Roncin, A. Le Floch, F. Launay, C. Letzelter, and J. Rostas, Reinvestigation of the vacuum ultraviolet spectrum of CO and isotopic species: The $B^1\Sigma^+ \leftrightarrow X^1\Sigma^+$ transition, J. Mol. Spectrosc. **121**, 309 (1987).

[7] R. Kępa, M. Ostrowska-Kopeć, I. Piotrowska, M. Zachwieja, R. Hakalla, W. Szajna, and P. Kolek, Ångström ($B^1\Sigma^+ \rightarrow A^1\Pi$) 0–1 and 1–1 bands in isotopic CO molecules: Further investigations, J. Phys. B At. Mol. Opt. Phys. **47**, 045101 (2014).

[8] S. J. Klippenstein, L. B. Harding, and B. Ruscic, *Ab initio* computations and active thermochemical tables hand in hand: Heats of formation of core combustion species, J. Phys. Chem. A **121**, 6580 (2017).

[9] G. Frenking, C. Loschen, A. Krapp, S. Fau, and S. H. Strauss, Electronic structure of CO: An exercise in modern chemical bonding theory, J. Comput. Chem. **28**, 117 (2007).

[10] N. Hölsch, M. Beyer, E. J. Salumbides, K. S. E. Eikema, W. Ubachs, C. Jungen, and F. Merkt, Benchmarking theory with an improved measurement of the ionization and dissociation energies of H_2, Phys. Rev. Lett. **122**, 103002 (2019).

[11] E. Eyler and N. Melikechi, Near-threshold continuum structure and the dissociation energies of H_2, HD, and D_2, Phys. Rev. A **48**, R18 (1993).

[12] A. Balakrishnan, V. Smith, and B. P. Stoicheff, Dissociation energies of the hydrogen and deuterium molecules, Phys. Rev. A **49**, 2460 (1994).

[13] Y. P. Zhang, C. H. Cheng, J. T. Kim, J. Stanojevic, and E. E. Eyle, Dissociation energies of molecular hydrogen and the hydrogen molecular ion, Phys. Rev. Lett. **92**, 203003 (2004).

[14] C. W. Zucker and E. E. Eyler, Photodissociation cross sections from the E, F state of H_2, J. Chem. Phys. **85**, 7180 (1986).

[15] J. D. D. Martin and J. W. Hepburn, Electric field induced dissociation of molecules in Rydberg-like highly vibrationally excited ion-pair state, Phys. Rev. Lett. **79**, 3154 (1997).

[16] J. Yang, Y. Hao, J. Li, C. Zhou, and Y. Mo, A combined zero electronic kinetic energy spectroscopy and ion-pair dissociation imaging study of the ($X\,^2\Pi_g$) structure, J. Chem. Phys. **122**, 134308 (2005).

[17] J. Li, Y. Hao, J. Yang, C. Zhou, and Y. Mo, Vibrational structure, spin-orbit splitting, and bond dissociation energy of studied by zero kinetic energy photoelectron spectroscopy and ion-pair formation imaging method, J. Chem. Phys. **127**, 104307 (2007).

[18] C. Kreis, U. Hollenstein, and F. Merkt, Threshold-ion-pair-production spectroscopy of H_2S and D_2S, Mol. Phys. **120**, 15 (2022).

[19] P. Erman, E. Raehlew-Kiillne, and S. L. Sorensen, Synchrotron radiation induced photoionization and photodissociation of carbon monoxide in the 14–35 eV region, Z. Phys. D. **30**, 315 (1994).

[20] M. D. Morse, Predissociation measurement of bond dissociation energies, Acc. Chem. Res. **52**, 119 (2019).

[21] E. P. Wigner, On the behavior of cross sections near thresholds, Phys. Rev. **73**, 1002 (1948).

[22] Y. Hatano, Interaction of VUV photons with molecules: Spectroscopy and dynamics of molecular superexcited states, J. Electron. Spectrosc. Relat. Phenom. **119**, 107 (2001).

[23] Y. Zhou, Q. Meng, and Y. Mo, Photodissociation dynamics of superexcited O_2: Dissociation channels $O(^5S)$ vs $O(^3S)$, J. Chem. Phys. **141**, 014301 (2014).

[24] G. R. Cook, P. H. Metzger, and M. Ogawa, Photoionization and absorption coefficients of CO in the 600 to 1000 Å region, Can. J. Phys. **43**, 1706 (1965).

[25] D. M. P. Holland and D. A. Shaw, A study of the valence shell absolute photoabsorption, photoionization and photodissociation cross sections, and the photoionization quantum efficiency of carbon monoxide, J. Phys. B At. Mol. Opt. Phys. **53**, 144004 (2020).

[26] L. Guan, P. Jiang, G. Zhang, T. Yin, M. Cheng, and H. Gao, Photodissociation branching ratios of $^{12}C\,^{16}O$ from 110 500 to 113 045 cm^{-1}: First observation of the $C(^1S)$ channel, Astron. Astrophys. **647**, A127 (2021).

[27] X. Shi, H. Gao, Q. Yin, Y. Chang, R. C. Wiens, W. M. Jackson, and C. Y. Ng, Branching ratio measurements of the predissociation of $^{12}C\,^{16}O$ by time-slice velocity-map ion imaging in the energy region from 106 250 to 107 800 cm^{-1}, J. Phys. Chem. A **122**, 8136 (2018).

[28] J. Wang, Q. Meng, and Y. Mo, Oscillation of branching ratios between the $D(2s) + D(1s)$ and the $D(2p) + D(1s)$ channels in direct photodissociation of D_2, Phys. Rev. Lett. **119**, 053002 (2017).

[29] T. J. B. Eppink and D. H. Parker, Velocity map imaging of ions and electrons using electrostatic lenses: Application in photoelectron and photofragment ion imaging of molecular oxygen, Rev. Sci. Instrum. **68**, 3477 (1997).

[30] J. E. Sansonetti and W. C. Martin, Handbook of basic atomic spectroscopic data, J. Phys. Chem. Ref. Data **34**, 1559 (2005).

[31] R. N. Zare and D. R. Herschbach, Doppler line shape of atomic fluorescence excited by molecular photodissociation, Proc. IEEE **51**, 173 (1963).

[32] S. J. Singer, K. F. Freed, and Y. B. Band, Cross sections and angular distributions for individual fragment fine structure

levels produced in one- and two-photon photodissociation of NaH, J. Chem. Phys. **81**, 3091 (1984).

[33] B. Leyh, J. Delwiche, M.-J. Hubin-Franskin, and I. Nenner, Electronic autoionization in carbon monoxide: The effects of the vibrational motion, Chem. Phys. Lett. **115**, 243 (1987).

[34] A. Ehresmann, S. Machida, M. Ukai, K. Kameta, M. Kitajima, N. Kouchi, Y. Hatano, K. Ito, and T. Hayaishik, Photodissociation of CO: Partial cross sections for neutral dissociative excitation, J. Phys. B At. Mol. Opt. Phys. **29**, 3629 (1996).

[35] Y. Zhao, K. Wang, L. Li, P. Huang, Q. Zeng, M. Gao, and L. Sheng, Study of photoionization mass spectrum of carbon monoxide from ionization threshold to 575 Å by using synchrotron radiation, J. Electron. Spectrosc. Relat. Phenom. **246**, 147032 (2021).

[36] P. Erman, A. Karawajczyk, E. Rachlew-Källne, C. Strömholm, J. Larsson, A. Persson, and R. Zerne, Direct determination of the ionization potential of CO by resonantly enhanced multiphoton ionization mass spectroscopy, Chem. Phys. Lett. **215**, 173 (1993).

[37] M. Evans and C. Y. Ng, Rotationally resolved pulsed field ionization photoelectron study of $CO^+(X^2\Sigma^+,\ v^+ = 0$–$42)$ in the energy range of 13.98–21.92 eV, J. Chem. Phys. **111**, 8879 (1999).

[38] M. Ogawa and S. Ogawa, Absorption spectrum of CO in the Hopfield helium continuum region, 600–1020 Å, J. Mol. Spectrosc. **41**, 393 (1972).

[39] S. L. Guberman, Potential energy curves for the dissociative recombination of CO^+, J. Phys. Chem. A. **117**, 9704 (2013).

[40] G. J. Vazquez, J. M. Amero, H. P. Liebermann, and H. Lefebvre-Brion, Potential energy curves for the $^1\Sigma^+$ and $^{1,3}\Pi$ states of $CO^\dagger$, J. Phys. Chem. **113**, 13395 (2009).